

Visualization of deflagration-to-detonation transitions in a channel with repeated obstacles using a hydrogen–oxygen mixture

S. Maeda¹ · S. Minami¹ · D. Okamoto¹ · T. Obara¹

Received: 31 October 2015 / Revised: 10 April 2016 / Accepted: 18 April 2016 / Published online: 6 May 2016
© Springer-Verlag Berlin Heidelberg 2016

Abstract The deflagration-to-detonation transition in a 100 mm square cross-section channel was investigated for a highly reactive stoichiometric hydrogen oxygen mixture at 70 kPa. Obstacles of 5 mm width and 5, 10, and 15 mm heights were equally spaced 60 mm apart at the bottom of the channel. The phenomenon was investigated primarily by time-resolved schlieren visualization from two orthogonal directions using a high-speed video camera. The detonation transition occurred over a remarkably short distance within only three or four repeated obstacles. The global flame speed just before the detonation transition was well below the sound speed of the combustion products and did not reach the sound speed of the initial unreacted gas for tests with an obstacle height of 5 and 10 mm. These results indicate that a detonation transition does not always require global flame acceleration beyond the speed of sound for highly reactive combustible mixtures. A possible mechanism for this detonation initiation was the mixing of the unreacted and reacted gas in the vicinity of the flame front convoluted by the vortex present behind each obstacle, and the formation of a hot spot by the shock wave. The final onset of the detonation origi-

nated from the unreacted gas pocket, which was surrounded by the obstacle downstream face and the channel wall.

Keywords Detonation wave · Deflagration wave · Deflagration-to-detonation transition (DDT) · Obstacle-filled channel · Schlieren visualization

1 Introduction

Combustion waves propagating in a combustible mixture can be classified as either deflagration or detonation waves. In an unconfined space, detonation waves are rarely initiated directly, unless extremely high-ignition energy is supplied to the combustible mixture. In a semi-confined tube or channel, a deflagration-to-detonation transition (DDT) [1, 2] produces the detonation wave through acceleration of the deflagration wave ignited by a small amount of ignition energy. The DDT process has great importance for practical applications, and for the determination of explosion hazards involved with a detonation wave. If a deflagration wave undergoes strong flame acceleration and the diameter of the channel is sufficiently large compared to the cell sizes of the detonation wave, a detonation wave can form producing high-pressure combustion products, even if the ignition source is weak. Therefore, the phenomena associated with the DDT process belong to the main topics for research concerning gaseous detonation. An early investigation by Urtiew and Oppenheim [3] showed multi-frame schlieren photographs observing the DDT process, in which the detonation wave was established instantaneously as the consequence of the localized explosion between the leading shock wave and turbulent flame front. The localized explosion requires a shock amplification process, e.g., the SWACER mechanism proposed by Lee [1], to establish the detonation wave; the induction time

Communicated by G. Ciccarelli.

This paper is based on work that was presented at the 25th International Colloquium on the Dynamics of Explosions and Reactive Systems, Leeds, UK, August 2–7, 2015.

Electronic supplementary material The online version of this article (doi:10.1007/s00193-016-0660-1) contains supplementary material, which is available to authorized users.

✉ S. Maeda
shinichi_maeda@mech.saitama-u.ac.jp

¹ Graduate School of Science and Engineering, Saitama University, 255 Shimo-Okubo, Sakura-ku, Saitama, Saitama 338-8570, Japan

gradient inside the volume of the unreacted but sensitized mixture is the dominant factor for the shock amplification. In a tube with a smooth inner wall, the distance from an ignition source to the point of detonation onset (DDT distance) is comparatively long. Inserting obstacles, such as a spiral coil (often known as a Shchelkin spiral [4]) or orifice plates, into the tube is known to significantly reduce the DDT distance. The role of the obstacles in the DDT process has widely been investigated [5–10] using fuel–air mixtures to establish the critical conditions for application to industrial safety. Flame propagation induces a flow of unreacted gas ahead of the flame, and the flow interacts with the obstacles inside the channel. As a result, the obstacles enhance the phase of global flame acceleration due to complex flow fields such as recirculation zones and turbulent shear layers produced behind obstacles [5,6]. The propagation regimes were classified as the quenching, slow-flame, fast-flame, and detonation (including “quasi-detonation”) regimes based on the measured terminal flame velocity in the tube with repeated orifice plates [7,8]. The enhanced flame acceleration shortened the distance needed to reach the critical flame speed, which was reported to be close to the sound speed of combustion products (around 1000 m/s), required for the final detonation transition. The numerical simulation of flame acceleration and detonation transition in the channel with repeated obstacles [9] showed that recirculation zones downstream of the obstacles result in an increase in the flame surface area and associated volumetric burning rate. The resulting high flame velocity, and the reflection of a sufficiently strong leading shock wave off the obstacles and channel walls creates a hot spot to trigger the detonation transition. Dorofeev et al. [10] suggested that the geometrical scaling of a channel with repeated obstacles required for the detonation onset was governed by the macroscopic size of a sensitized mixture. The role of the obstacles on the flame acceleration process and the final onset of detonation in the tube or channel filled with obstacles was investigated by several researchers [5–10]. The flame acceleration process is highly influenced by the channel boundary conditions and combustible mixture properties. In fuel and air mixtures, the flame acceleration process takes place over relatively long distances because of the lower mixture reactivity compared to fuel–oxygen mixtures. On the other hand, the final phase of detonation onset is considered to be a universal condition regardless of initial conditions [1,2,11]. In experimental investigations, resolving the final stage of DDT in detail is a difficult task, because of temporal and spatial measurement resolution limitations. In recent years, numerical simulations [11,12] were conducted for investigating the origin of the onset of detonation; furthermore, the mechanisms for creating hot spots and gradients of reactivity in the unreacted gas leading to the detonation transition were discussed.

Recently, Obara et al. [13] investigated the DDT process inside a rectangular channel equipped with repeated obstacles in a hydrogen–oxygen mixture. The channel had an inner cross section of 100 mm width and 85 mm height, and the repeated obstacles were mounted on the bottom wall of the channel. The spacing of the obstacles was chosen as 20, 40 or 60 mm, while the height of the obstacles was kept as 15 and 25 mm, respectively (the corresponding blockage ratios were 0.18 and 0.29). Initial pressures of a stoichiometric hydrogen–oxygen mixture were also varied between 30, 50, and 70 kPa. They optically observed the evolution of the flame and the leading shock wave using multi-frame schlieren photography. For the 60 mm obstacle spacing, they showed that detonation transition occurred via a local explosion between the obstacles after the flame propagated over several obstacles. The DDT distance was about 2.5 times the channel width, and the result showed that the required condition for detonation onset was achieved in a very short distance. They proposed that the shock–flame interaction between the obstacles was a contributing factor for the detonation onset. The shock wave was driven by the flame acceleration because the flame was convoluted by the vortex induced behind the obstacles, and the shock wave interacted with the flame after reflecting off the channel wall and the adjacent obstacle.

The present study focuses on how the detonation transition occurs in such a short distance when a channel with repeated obstacles is filled with a highly reactive mixture, such as stoichiometric hydrogen and oxygen. The present study was carried out in a channel with repeated small obstacles, specifically for the case in which the blockage ratios were less than 0.2. The small obstacles strongly enhanced the detonation transition when the highly reactive mixture was used [13]; nevertheless, such small obstacles would have minimal effect on the flame acceleration process when a fuel–air mixture is used at around atmospheric pressures [2]. This investigation concerning the strong effect of the obstacles on the DDT distance, even when the obstacles are small, will have great importance with respect to detonation hazards and practical applications of detonations. If a small obstacle can cause a short DDT distance in a highly reactive mixture, the local contributing phenomena in the vicinity of the obstacle will be necessary for the detonation transition, rather than the global flame acceleration reaching the critical flame speed. An unreacted gas pocket surrounded by the flame front is created just behind the obstacle when the flame propagates over the obstacle. The entrainment of the unreacted gas by the combustion products may induce a rapid reaction in the unreacted gas pocket behind the obstacle. This rapid reaction in the highly reactive mixture may contribute to the detonation onset even if the flame speed is slower than the “critical flame speed”. It is known that a strong jet of combustion products may directly initiate the detonation wave in

the unreacted gas, commonly referred to as “jet initiation” [14–16]. In jet initiation, turbulent mixing between the unreacted gas and combustion products is induced by the vortex on the boundary between the static unreacted gas and the highly accelerated flame jet. The factors affecting the detonation initiation are the geometrical scale of the turbulent mixing and the length scale of the chemical reaction. The required condition for direct initiation was expressed in terms of the orifice diameter for the flame jetting and the detonation cell width of the combustible mixture. The present paper discusses several possible factors that contribute to the short DDT distance, including the above-mentioned rapid reaction behind the obstacle. The experiments were carried out primarily by time-resolved schlieren visualization of the DDT phenomena using a high-speed video camera. Visualization from two orthogonal directions was conducted to discuss the three-dimensional spatial evolution of a deflagration wave behind an obstacle and the final stage of detonation onset. The aim of the present study is to highlight a mechanism for detonation onset when there is insufficient flame acceleration to reach supersonic speed.

2 Experimental setup and condition

Figure 1 shows a schematic of the experimental setup. The combustion channel of 580 mm length was connected to a dump tube of 4 m length. The inner cross section of the channel was 100 mm wide and 100 mm high. A plate of 15 mm thickness was installed along the entire length of the bottom wall, and thus the inner cross section of the channel became 85 mm high by 100 mm wide. Each obstacle was 5 mm wide with height h . The spacing between the obstacles was 60 mm, defined as the distance between the upstream faces of adjacent obstacles. The first obstacle was placed 20 mm downstream from the end wall, where a spark plug was mounted. The combustion channel and the dump tube

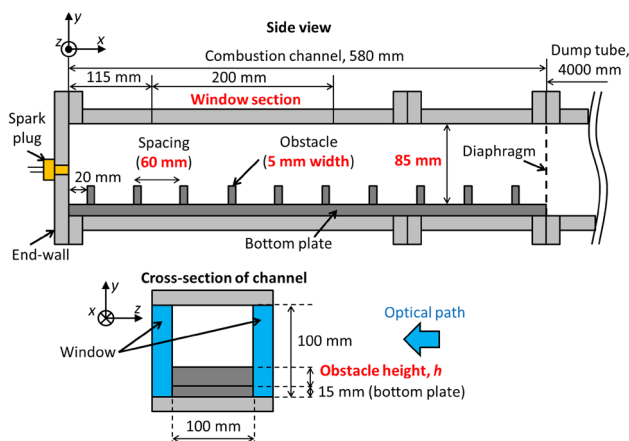


Fig. 1 Experimental setup

Table 1 Experimental condition

Test gas	Repeated obstacles		
	Spacing (mm)	Width (mm)	Height, h (mm)
$2\text{H}_2 + \text{O}_2$, 70 kPa, room temp.	60	5	5
			10
			15

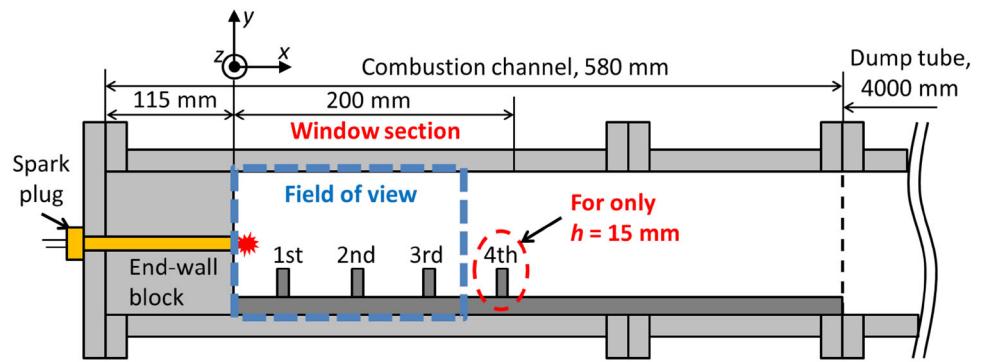
were separated by inserting a thin diaphragm of 25 μm thickness. The dump tube was evacuated prior to a test, and the combustion channel was filled with a combustible mixture. For optical access, a pair of glass windows of 200 mm width and 100 mm height was installed in the combustion channel. The coordinates were set so that the x direction pointed downstream along the channel axis and the origin was at the ignition point, as shown in Fig. 1. The location of the window section was between $x = 115$ –315 mm. The spark energy used for ignition of the combustible mixture was not measured in the present study; however, the energy was of the order of several millijoules, typical of a conventional automotive ignition system and spark plug (with a spark gap of about 1 mm). A conventional double-mirror Z-configuration schlieren system was used for the visualization of the flow field. An iris diaphragm was used as the schlieren knife edge, and the light source image was cut circularly from the outer circumference to the center.

The experimental conditions are listed in Table 1. The test gas used to fill the combustion channel was a stoichiometric hydrogen–oxygen mixture, and the initial pressure was 70 kPa for all tests. The mixture was prepared in a mixture tank using the method of partial pressure, and transferred to the combustion channel from the mixture tank. The uncertainty of the pressure measurement associated with the combustion channel and the mixture tank was ± 2 kPa. The error of the equivalence ratio of the mixture owing to the accuracy uncertainty of the pressure measurement was ± 0.05 . The initial temperature of the mixture was 293 ± 5 K including the uncertainty of the thermocouple. The heights of the obstacles used were 5, 10, and 15 mm, and the corresponding blockage ratios were 0.06, 0.12, and 0.18, respectively.

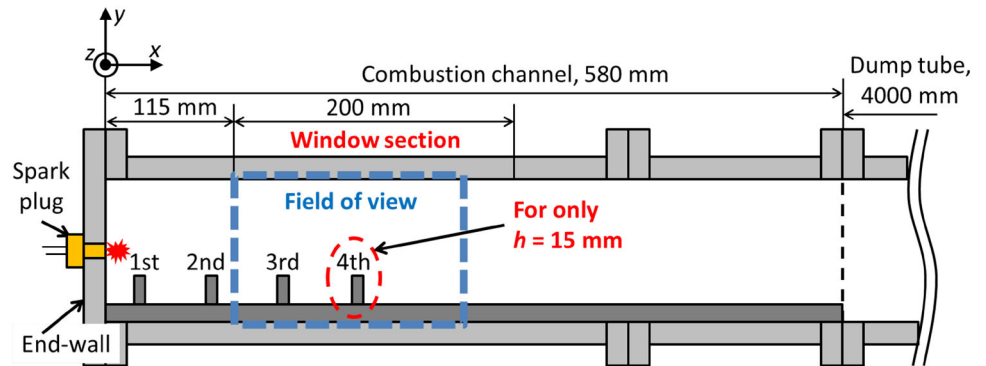
As a preliminary experiment ahead of the flow visualizations, the soot-foil method was applied for an estimation of the DDT distance. The soot foils were placed at the window section. When conducting the flow visualizations, we removed the obstacles downstream of the detonation transition to investigate whether the downstream obstacles affected the location of the detonation transition. Therefore, only three or four obstacles were used.

The flow visualization in the side view was conducted in two regions: near the ignition region and in the downstream region, as shown in Fig. 2a, b, respectively. In the visual-

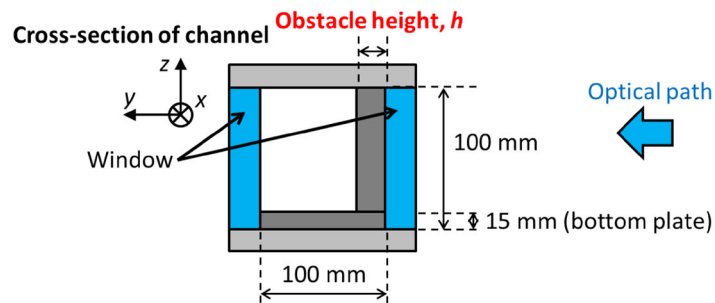
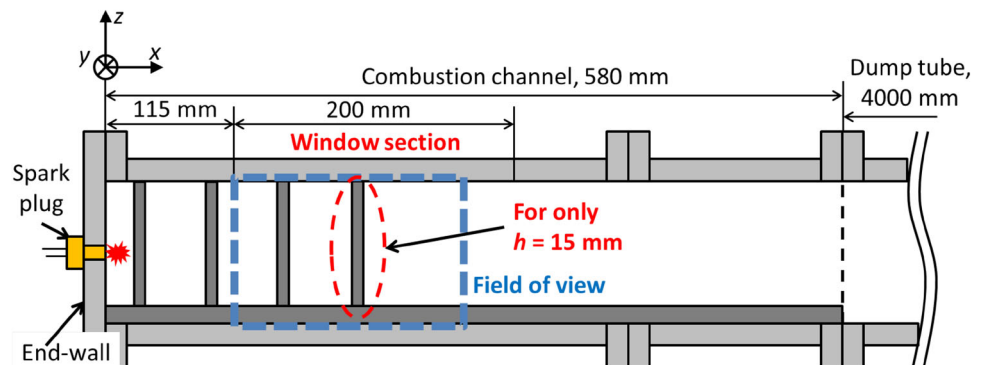
Fig. 2 Experimental setup for flow visualization study



(a) Side-view near ignition region



(b) Side-view in downstream region



(c) Bottom-view in downstream region

ization near the ignition region, an extended spark plug was placed through an end-wall block so that the spark point was located inside the window section. The window section was between $x = 0\text{--}200$ mm in Fig. 2a. The field-of-view was between $x = 0\text{--}160$ mm because of the limited size of the collimated light, and ranged from the ignition point to the third obstacle. A high-speed video camera (Phantom v7.3, Vision Research, Inc.) was used for time-resolved recordings, with an inter-frame time of $16.5\ \mu\text{s}$ and an exposure time of $1\ \mu\text{s}$. The spark plug was at the end wall, similar to that shown in Fig. 1 in the visualization of the downstream region. The field-of-view was between $x = 120\text{--}270$ mm, and ranged from the third obstacle to the downstream region. In this visualization, another high-speed video camera (Ultra Cam HS-106E, nac Image Technology, Inc.) was used for a better temporal resolution of the detonation onset, with an inter-frame time of $2\ \mu\text{s}$ and an exposure time of $100\ \text{ns}$. In the downstream region, the flow field was also visualized by changing the direction of the visualization, as shown in the bottom view in Fig. 2c. The ignition point and field-of-view were the same as those in Fig. 2b; however, the DDT process was visualized from the bottom. As shown in the schematic, the obstacles were mounted on the bottom plate so that the bottom surface of the obstacle was on the glass window. This setup was similar to that used by Johansen and Ciccarelli [6].

3 Results and discussion

3.1 DDT distance

Experiments using the soot-foil method were first conducted for estimating the location of the detonation transition. In these preliminary experiments, the repeated obstacles were installed along the entire length of the combustion channel. The typical soot-foil record obtained for $h = 5$ mm is shown in Fig. 3, where the direction of flame propagation is from right to left. From Fig. 3, the origin of the detonation transition appeared to be near the downstream face of the third obstacle, corresponding to the origin of the fine cellular pattern (i.e., the dotted circle in Fig. 3). Similar soot-foil records were obtained for all heights of the obstacles. The detonation transition occurred behind the third obstacle for the case of $h = 5$ and 10 mm and behind the fourth obstacle for the case of $h = 15$ mm. The smaller obstacle led to a shorter DDT distance in the present experiments. A larger obstacle normally produces stronger flame acceleration when a fuel–air mixture is used for blockage ratios below 0.2 . The present results indicate that the obstacle height plays an important role in the actual detonation initiation process. The preliminary experiments using the soot-foil method were repeated three times for all the obstacle heights. The reproducibility of the location of the detonation transition for each obstacle height was con-

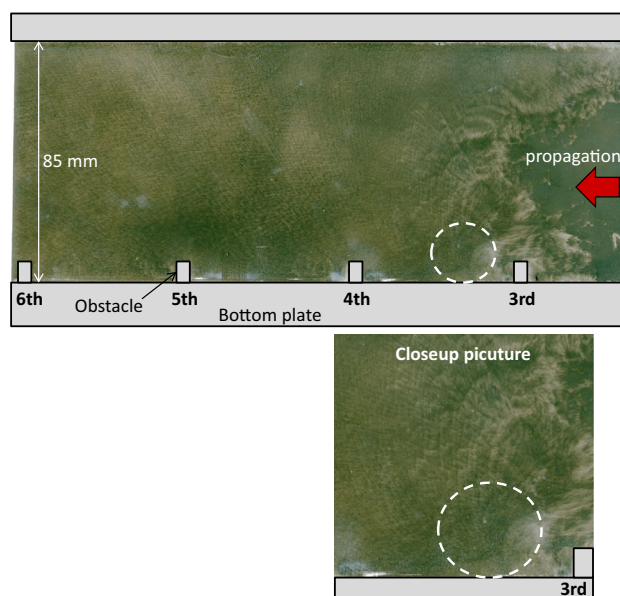


Fig. 3 Typical soot-foil record obtained at window section. The height, width, and spacing of obstacles were 5 , 5 , and 60 mm, respectively. The test gas was a stoichiometric hydrogen–oxygen mixture of 70 kPa. The dotted circle shows the region in which the fine cellular pattern originates

firmed in these repeated experiments. The third and fourth obstacles were placed 140 and 200 mm downstream from the ignition point, respectively. The obtained DDT distances were considerably shorter compared with the results using the same combustion channel without the obstacles where DDT occurred at distances between about $1.0\text{--}1.5$ m.

Dorofeev et al. [10] suggested that a characteristic geometrical length L was required for a detonation transition inside a channel with repeated obstacles. This length L was defined as $L = S/(1 - d/H)$, where S was the spacing between two opposite faces of adjacent obstacles, H was the channel height, and d was the open channel height above the obstacles. In our experiments, these parameters were $S = 55$ mm, $H = 85$ mm, and $d = 80, 75,$ and 70 mm for the obstacle heights of $5, 10,$ and 15 mm, respectively. Dorofeev et al. showed that the detonation transition required the minimum value of L to be seven times the detonation cell width of the test gas ($L \geq 7\lambda$). In the present experiment, the channel height was large compared to the obstacle height, and the test gas was a stoichiometric hydrogen–oxygen mixture, which is highly reactive compared to a fuel–air mixture. The cell width of the unreacted gas was around 2 mm [17, 18]. Therefore, the value of L was extremely high at $156, 234,$ and 468 times the cell width for the case of $h = 15, 10,$ and 5 mm, respectively. The results of the present study were consistent with the $L \geq 7\lambda$ criterion of Dorofeev et al. [10] for the condition of the detonation transition, because the values of L satisfied the criterion by a large factor.

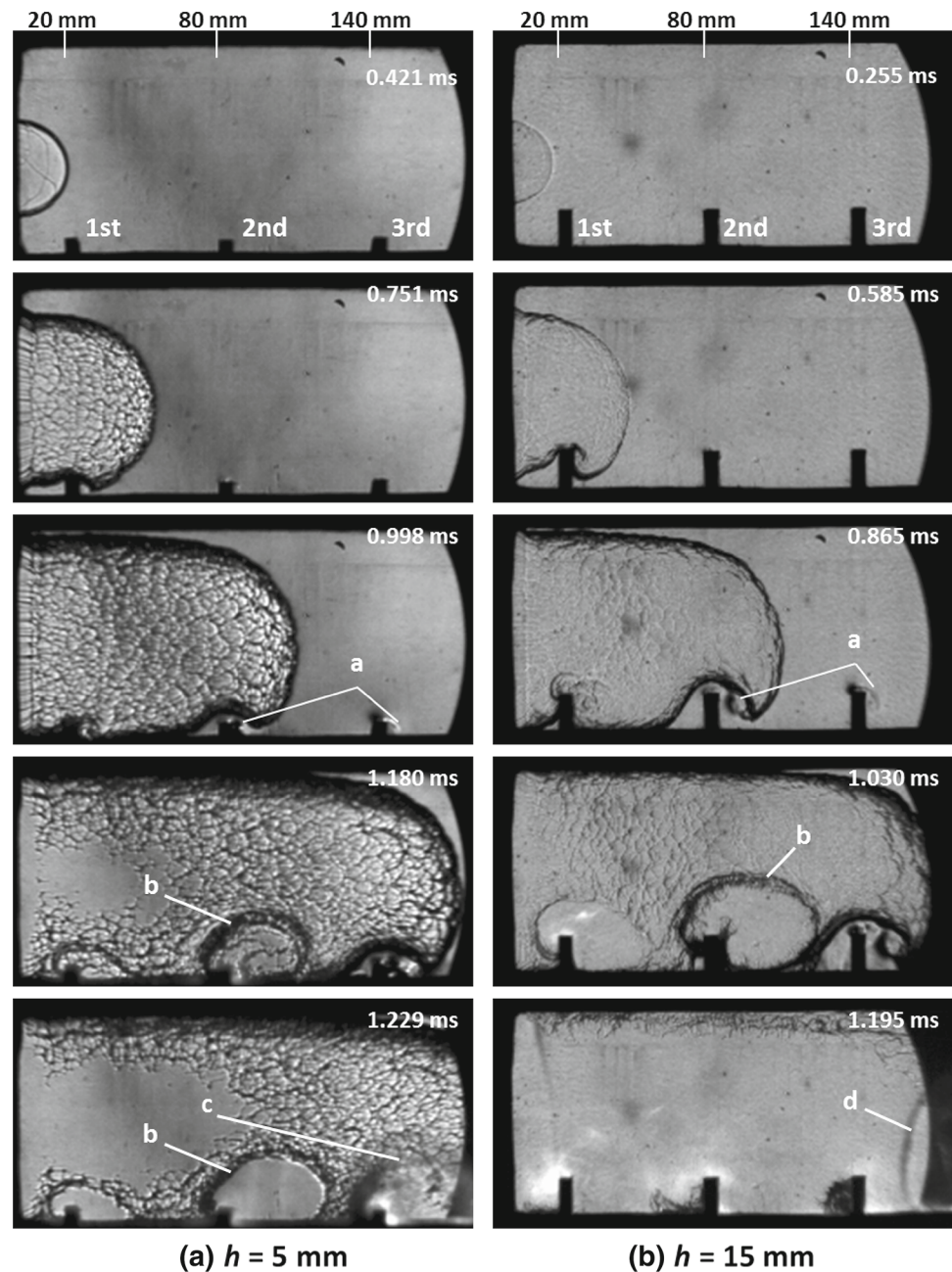
3.2 Visualization of flame evolution near ignition region

Figure 4 shows the schlieren images for tests with obstacle heights: (a) $h = 5$ mm and (b) $h = 15$ mm, obtained at the ignition region as shown in Fig. 2a. The time indicated on each frame is the elapsed time from the triggering of the ignition circuit. Note that the time intervals between shown frames are not constant. The electrode for ignition was located on the left wall, and the first to third obstacles were visible inside the field of view. Figure 5 shows the flame tip velocities along the channel axis measured from the schlieren images in Fig. 4. The sound speed of

the initial unreacted gas and the locations of each obstacle are also shown in the figure. Measurements of the flame tip velocity were conducted by manually extracting locations of the leading edge of the flame tip from the time-series schlieren images. Considering the accuracy for detecting the location of the flame tip, owing to the spatial resolution of each schlieren image, the error of the flame tip velocity was ± 30 m/s. Experiments for the $h = 5$ and 10 mm tests were repeated twice to confirm the reproducibility of the flame evolution.

In the first frames of Fig. 4a, b, the hemispherical flame expanded from the ignition point. In this early stage, the flame

Fig. 4 Schlieren images for two obstacle heights obtained near the ignition region (side view). The test gas was a stoichiometric hydrogen–oxygen mixture at 70 kPa. The time indicated on each frame is the elapsed time from ignition. Ignition is on the left wall. *a* Vortex induced behind the obstacle, *b* volumetric explosion behind the obstacle, *c* detonation wave, *d* retonation wave



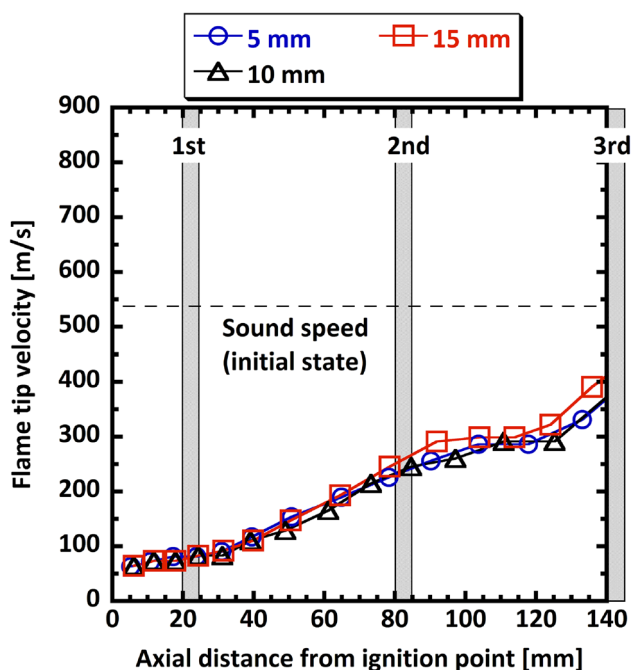


Fig. 5 Flame tip velocity along channel axis near the ignition region. The test gas was a stoichiometric hydrogen–oxygen mixture of 70 kPa

front seemed to be smooth and laminar. The propagation velocity of the laminar flame viewed from a laboratory coordinate is typically approximated by the product of the laminar flame speed and the expansion ratio (density ratio of reacted and unreacted gases), calculated to be about 80 m/s in this case. This estimated flame velocity was consistent with the measured value at the early stage, as shown in Fig. 5. A cellular structure [2] developed by the time the flame approached the first obstacle (second frame in Fig. 4a, b). This cellular structure is due to the thermal-diffusive instability and/or the hydrodynamic instability (Landau–Darrieus instability). The Lewis number was calculated to be 0.35 for the stoichiometric hydrogen–oxygen mixture, if the hydrogen was regarded as the deficient reactant, and thus this condition would support the development of the cellular flame. Another factor for the development of the cellular flame is associated with the large Peclet number, which was defined as the ratio of the flame radius to the flame thickness, as reported in the investigations [19, 20] related to spherical flame propagation. The radius of the expanded flame was considerably larger than the flame thickness of the highly reactive mixture used in the present study, and thus the cellular flame may develop relatively early after the ignition. The flame front quickly distorted when the flame passed the first obstacle, and consumed the unreacted gas behind the obstacle. As shown in Fig. 5, the global flame speed gradually increased as the flame passed the obstacles, and the initial flame acceleration showed almost the same pattern for $h = 5, 10,$ and 15 mm. The flame propagation induced the displacement flow

of unreacted gas, producing vortices “a” downstream of the second and third obstacles in the third frames of Fig. 4a, b. As the vortices developed behind the obstacles, diffraction of the flame around the second and third obstacles became larger in scale, compared to that observed around the first obstacle. As a result, this created the larger unreacted gas pockets behind the second and third obstacles. The fourth and fifth frame of Fig. 4a showed that the curved line “b” corresponding to a density interface developed over time behind the second obstacle. The flame front behind the obstacle is highly curved and the schlieren images represent the integration of the density gradient along the obstacle depth. Although the schlieren images are of insufficient quality to definitively identify the phenomenon progressing behind the obstacle in detail, they indicate that a volumetric explosion presumably occurs behind the obstacle. Wrinkles are visible on the surface of the main flame front in the region outside the curved line “b” and thus the unreacted gas remains between the flame surface and the optical window. The wrinkles are also visible in the region inside the curved line “b” in the fourth frame of Fig. 4a. On the other hand, the wrinkles are not visible in the region inside the curved line “b” in the fifth frame of Fig. 4a and thus the flame front is already attached to the optical window. This indicates that a rapid reaction progressed in the unreacted gas pocket behind the obstacle between the fourth and the fifth frame. In the fourth frame of Fig. 4b, the flow pattern behind the second obstacle is similar to that in the fifth frame of Fig. 4a, which indicates a rapid reaction in the unreacted gas pocket. The schlieren images indicating such a volumetric explosion were observed behind the second and third obstacles for all obstacle heights. After the flame passed the third obstacle, a detonation wave “c” was initiated in the fifth frame of Fig. 4a most likely originating in the unreacted gas pocket. The detonation front appears blurred because of the relatively long exposure time of 1 μ s. In the fifth frame of Fig. 4b, a strong shock wave “d” propagated back in the upstream direction in the reacted gas. This shock wave, commonly referred to as a “retonation wave”, indicates that detonation transition occurred downstream of the field-of-view. From Fig. 5, the flame tip velocities were estimated to be about 400 m/s at the third obstacle for all obstacle heights. Therefore, the global flame speed was still subsonic (the speed of sound in the unreacted gas is 530 m/s) in this field-of-view, corroborated by the fact that no compression waves were observed ahead of the flame in the schlieren photographs. In both cases of Fig. 4a, b, the position of the detonation transition was consistent with the soot-foil record shown in the previous section, in spite of the removal of the downstream obstacles. However, the temporal resolution and the field-of-view were insufficient to capture the final process of the detonation transition. Better visualization focusing on this final stage of DDT is provided in the next section.

3.3 Visualization of flame evolution at downstream region (side view)

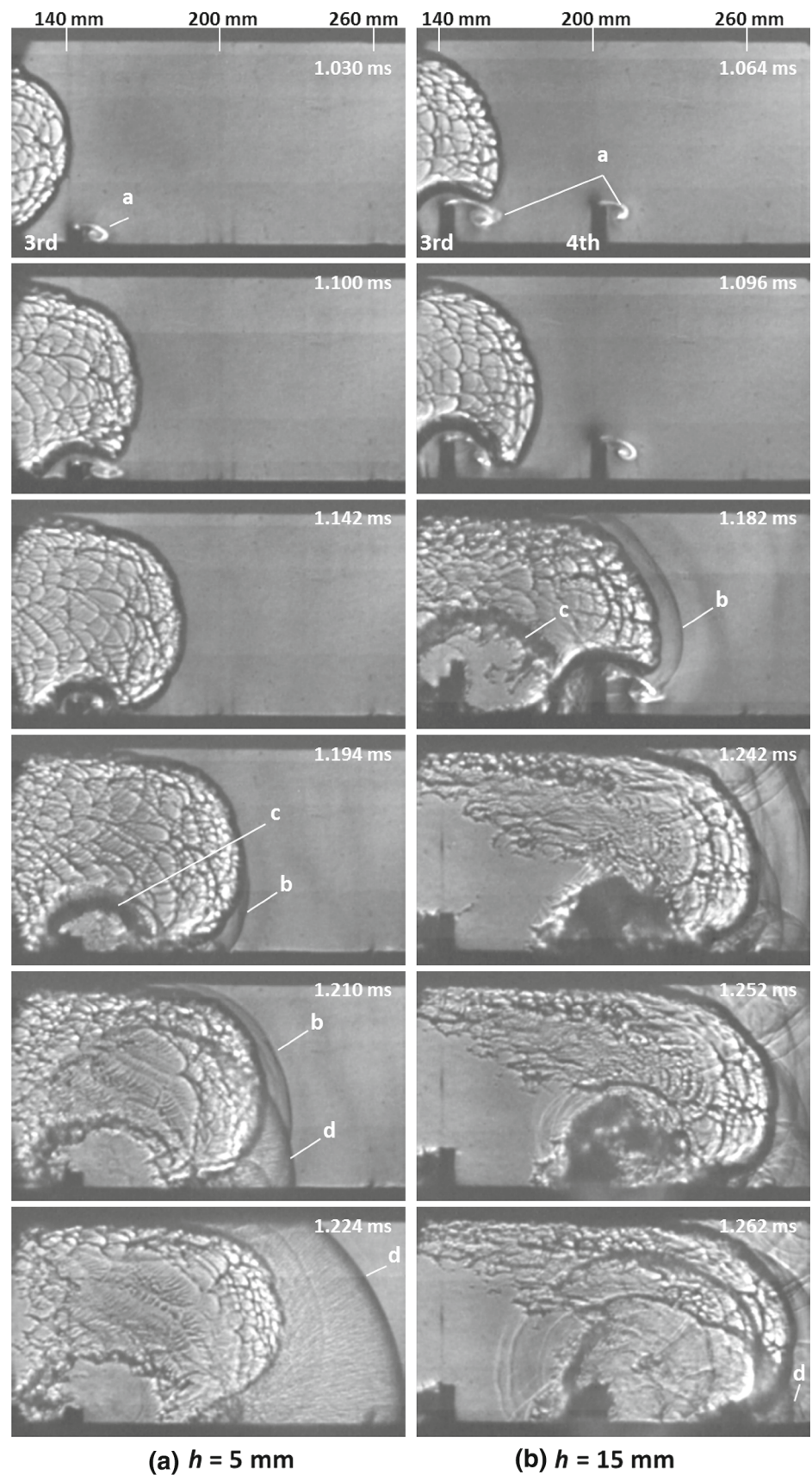
Figure 6 shows the multi-frame schlieren images for the two obstacle heights: (a) $h = 5$ mm and (b) $h = 15$ mm, obtained at the downstream region as shown in Fig. 2b (the full time-resolution videos are attached as supplementary material). Only the third obstacle is visible in the sequence of images included in Fig. 6a, and the third and fourth obstacles are visible in Fig. 6b. In both experiments, the vortices “a” had already developed behind the obstacle in the first frame. The flame passed the third obstacle in the second and third frames of Fig. 6a and in the first and second frames of Fig. 6b. The fourth frame of Fig. 6a shows evidence of a volumetric explosion “c” behind the third obstacle, as described in the previous section. In Fig. 6a, the shock wave “b” forms ahead of the flame front in the fourth and fifth frames, and the expanding fast wave “d” also forms in the fifth and sixth frames. The propagation velocity of this fast wave, estimated from the schlieren images, is over 3000 m/s; this velocity is slightly higher than the Chapman–Jouguet velocity (about 2820 m/s) of the initial unreacted gas. This wave represents an overdriven detonation wave. The origin of the detonation wave was estimated from the center of the curved detonation “d” to coincide with the unreacted gas pocket behind the third obstacle. A similar temporal evolution was observed in the case of $h = 10$ mm. In Fig. 6b, the third frame showed that the volumetric explosion “c” occurred after the flame surrounded the unreacted gas behind the third obstacle; however, this explosion did not trigger the detonation initiation. In the same frame, the flame passed the fourth obstacle and the leading shock wave “b” was generated ahead of the flame. An expanding detonation wave “d” propagating with a velocity of 3000 m/s is visible in the last frame. This detonation wave originated from the unreacted gas pocket behind the fourth obstacle. Based on the images in Fig. 6, the detonation transitions occurred at the same locations as those inferred from the soot-foil experiments in which the obstacles were installed along the entire length of the combustion channel. This indicates that the presence of the downstream obstacles has no effect on the detonation transition for these experimental conditions.

Figure 7 shows the measured flame tip velocity along the channel axis measured from the multi-frame schlieren images. The global flame speed is below the sound speed of unreacted gas (530 m/s) when the detonation wave was initiated in Fig. 6a (behind the third obstacle), and exceeded the sound speed in Fig. 6b (behind the fourth obstacle). The propagation velocity of the leading shock wave (“b” in Fig. 6a, b) was estimated to be around 1100 m/s from the schlieren movies, and the Mach number was around 2.1 when the sound speed of the unreacted gas is used. This value is a slight overestimation because the flow velocity of

the unreacted gas is not taken into account. The strength of the leading shock wave is such that it cannot be neglected. This leading shock wave reflects off the bottom wall of the channel because the shock wave is curved. This shock reflection can be observed in the fourth frame of Fig. 6a. The numerical simulation of Gamezo et al. [9] indicated that the reflection of the downstream obstacle and the Mach stem created by the shock reflection on the channel wall were a possible mechanism for the creation of the hot spots that can lead to detonation transition. The leading shock wave “b” in Fig. 6b was driven by the flame acceleration when the flame passed the fourth obstacle [13]. This is because the flame tip velocity became supersonic in this phase, as shown in Fig. 7, forming a shock wave ahead of the flame front. On the other hand, the origin of the shock wave “b” in Fig. 6a is not so obvious. The flame tip velocity was still subsonic in this phase, as shown in Fig. 7, and the shock wave seemed to propagate out from inside of the main flame front. The possible origins would be the volumetric explosion “c” behind the third obstacle, or that behind the second obstacle. However, the origin cannot definitively be identified from the schlieren images obtained in the present study. Figure 6a, b shows that the detonation transition occurred when a leading shock wave was generated. The mechanism leading to the detonation transition is associated with the volumetric explosion in the unreacted gas pocket behind the obstacle and/or the generation of a hot spot by the shock reflection. Because the volumetric explosion “c” behind the third obstacle in Fig. 6b, without a leading shock wave present, could not trigger detonation onset, the presence of the leading shock wave also played an important role for the detonation transition in this condition. The DDT process observed in Fig. 6 would indicate that the unreacted gas pocket formed behind the obstacle had the important role of promoting the rapid reaction arising from the mixing of the unreacted and reacted gases. The turbulent mixing between the unreacted gas and the jet of combustion products may directly initiate the detonation wave in the process of jet initiation [14–16]; however, it is difficult to determine whether solely turbulent mixing is sufficient for the DDT process observed in the present study.

The flame tip velocity, shown in Fig. 7, was well below the sound speed of combustion products under isobaric combustion (1370 m/s from the chemical equilibrium software, CEA [21]), which is the critical flame speed for detonation transition observed in many general fuel–air mixtures. The experimental investigation [22], using a smooth tube filled with a hydrogen–oxygen mixture, reported a flame speed of about 800 m/s before the transition to detonation, which is slower than the sound speed of combustion products. The flame speed observed in the present study was slower than that observed in a smooth tube case. In the case of $h = 5$ and 10 mm, the flame tip velocity did not reach the sound speed

Fig. 6 Multi-frame schlieren images for two cases of obstacle heights, h obtained in the downstream region (side view). The time indicated on each frame is an elapsed time from triggering the ignition circuit. The test gas was a stoichiometric hydrogen–oxygen mixture of 70 kPa. *a* Vortex behind the obstacle, *b* shock wave, *c* volumetric explosion behind the obstacle, *d* detonation wave



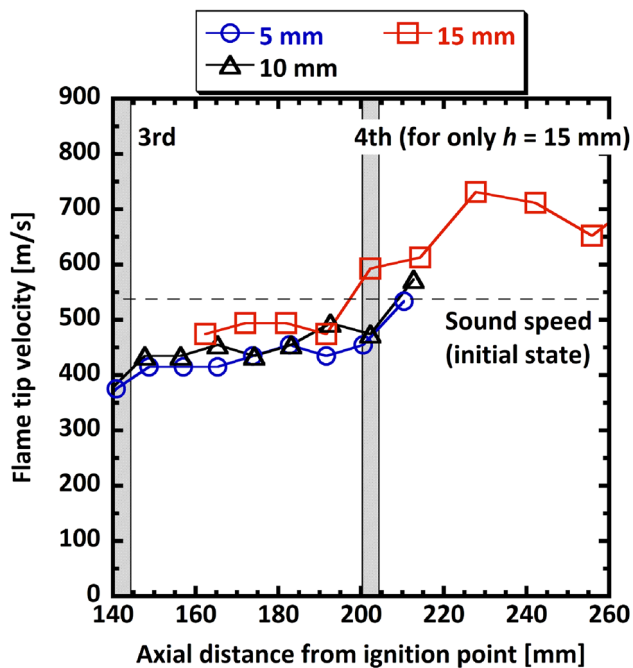


Fig. 7 Flame tip velocity along channel axis in the downstream region. The test gas was a stoichiometric hydrogen–oxygen mixture of 70 kPa

of the initial unreacted gas. These results demonstrate that a detonation transition does not always need global flame acceleration beyond the sound speed if the obstacle-filled channel is filled with highly reactive combustible mixtures such as hydrogen and oxygen.

The spacing between obstacles must be large enough to create a pocket of unreacted mixture of sufficient volume for the DDT process to occur, as observed in the present study. Obara et al. [13] conducted experiments with a 20 mm spacing between obstacles, which is shorter than that in the present study, and obstacle heights of 15 and 25 mm inside a similar rectangular channel (85 mm height by 100 mm width) as that used in the present study. In those experiments, the obstacle spacing was comparable to the obstacle heights, whereas in the present experiments the heights of the obstacles are more representative of wall roughness. They found that the local explosion did not occur between the obstacles because the scale of the vortex and the volume of unreacted gas between the obstacles was smaller compared to those of the case of discretely arranged obstacles in which the obstacle spacing was large enough to create a sufficient scale of the vortex and the unreacted mixture pocket behind the obstacle. Instead, they showed that an accumulation of weak shock waves ahead of the flame triggered detonation transition. They also indicated that the DDT distances in the channel with such closely spaced obstacles tended to become longer than that in the channel with discrete obstacles.

3.4 Visualization of flame evolution at downstream region (bottom view)

The detonation transition occurred as a localized phenomenon behind the obstacles. In this section, the flow visualizations of the bottom view (Fig. 2c) are shown. The bottom view shows the evolution of phenomena along the channel depth which could not be visualized in Fig. 6. Figure 8 shows the multi-frame schlieren images of the bottom view for the same conditions as those in Fig. 6 (the full time-resolution videos are attached as supplementary material). The first frame of Fig. 8a was chosen so that the position of the flame front closely matched the third frame of Fig. 6a. The flame passes the third obstacle in the first and second frames of Fig. 8a, where the region “a” roughly corresponds to the tip of the rolled-up flame behind the obstacle. An unreacted gas pocket is formed between the rolled-up flame and the downstream face of the third obstacle, as shown in the third frame of Fig. 6a. In the third and fourth frames of Fig. 8, a new region of a density gradient “b” overlaps the main flame, and the region develops between these frames. For showing the detailed temporal evolution, Fig. 9 shows the schlieren images of this phase of propagation in a higher frame-rate time sequence. The time range is from 1.136 to 1.164 ms, and the time interval is 4 μ s between each image. The region “a” in the first frame roughly corresponds to the tip of the rolled-up flame, as is similar to the second frame of Fig. 8a. The new region of the density gradient “b” (corresponds to the region “b” in Fig. 8a) develops over time into the vertical direction of the schlieren image near the downstream face of the third obstacle during 1.136–1.160 ms. The location where the region “b” is formed cannot be definitively identified from Fig. 9, because the schlieren image obtained from the bottom view is the superposition of the density gradients along the y direction in Fig. 2c. Additionally, the origin of region “b” is less apparent owing to the limited spatial resolution of the schlieren image. However, region “b” was assumed to correspond to the volumetric explosion in connection with the side view of Fig. 6a, because the fourth frame of Fig. 6a indicates that the volumetric explosion occurs near the downstream face of the third obstacle and another distinguishing reaction is not observed along the direction of the channel height (the y direction in Fig. 2b) except for the main flame front. The region of the density gradient “b” in Fig. 9 presumably expanded in the unreacted gas pocket behind the third obstacle during 1.136–1.160 ms, and was assumed to be a rapid reaction compared with the main flame front (the tip of the main flame front did not progress very much during this short period in Fig. 9). The fast wave “c” propagating along the top wall was observed in the last frame (1.164 ms) of Fig. 9. This fast wave corresponds with the wave front “c” in the fifth and sixth frame of Fig. 8a. This wave represents an overdriven detonation wave because the propagation velocity

Fig. 8 Multi-frame schlieren images for two cases of obstacle heights, h obtained in the downstream region (bottom view). The time indicated on each frame is an elapsed time from triggering the ignition circuit. The test gas was a stoichiometric hydrogen–oxygen mixture of 70 kPa. *a* Convoluted flame front behind the obstacle, *b* region progressing the rapid reaction, *c, d, g* detonation wave, *e* Vortex induced behind the obstacle, *f* shock wave

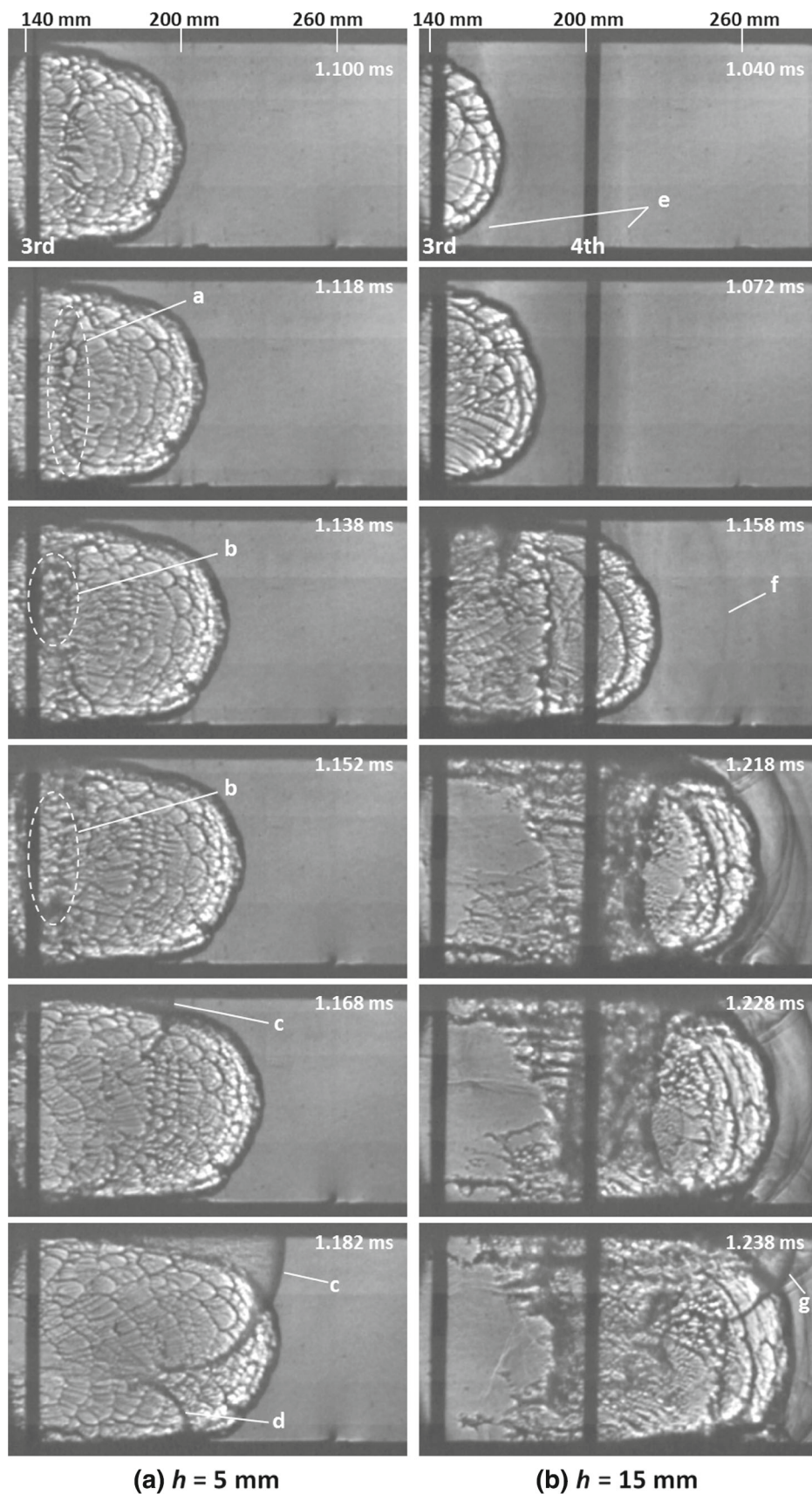
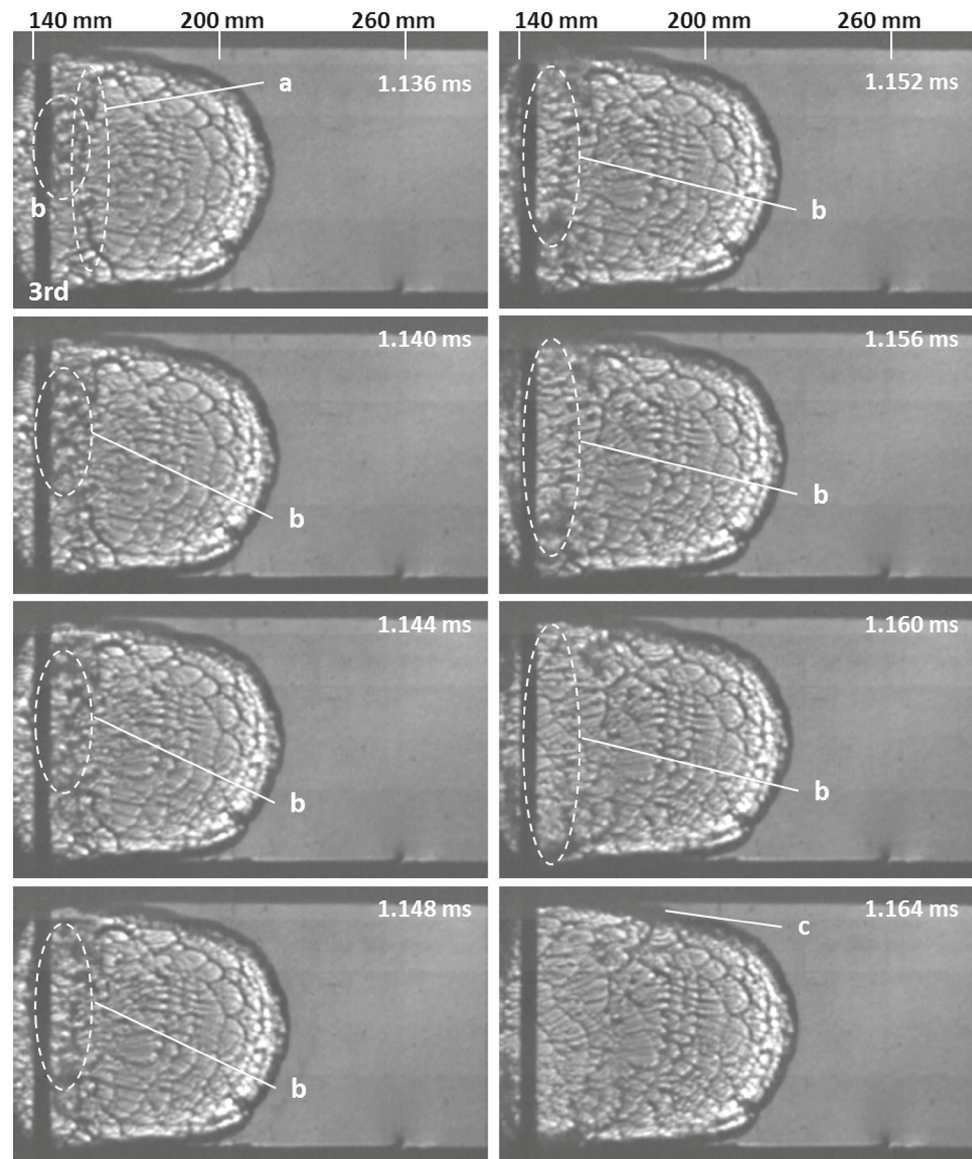


Fig. 9 Multi-frame schlieren images during the rapid reaction in the unreacted gas pocket behind the third obstacle (obstacle height, $h = 5$ mm), obtained in the downstream region (bottom view). The time indicated on each frame is an elapsed time from triggering an ignition circuit. The test gas was a stoichiometric hydrogen–oxygen mixture of 70 kPa. *a* Convoluted flame front behind the obstacle, *b* region progressing the rapid reaction, *c* detonation wave



is over 3000 m/s between the frames. The detonation wave originates from the top wall downstream of the third obstacle, as deduced from the center of the hemi-spherically expanding detonation wave. The precise location and time of the detonation onset could not be identified in the present study because the apparent luminescence associated with the detonation onset could not be observed; furthermore, the spatial resolution of the images was limited. In the lower position of the sixth frame in Fig. 8a, the detonation wave “d” was slightly retarded relative to the detonation wave at the upper position, because the rapid reaction seemed to expand in a slightly delayed manner in the lower direction in Fig. 8. A similar temporal evolution of the flame front was also observed in the case of $h = 10$ mm (no images shown here). Video images captured for tests with $h = 15$ mm are shown in Fig. 8b. The first frame was chosen so that the position of

the flame front is almost in accordance with that in the first frame of Fig. 6b, and the time intervals between each frame also coincide with those of Fig. 6b. The bright line “e” is probably associated with the vortex behind the obstacle. The complex system of the leading shock wave was observed after the flame passed the fourth obstacle. The expanding detonation wave “g” propagated along the top wall in the last frame (1.238 ms) of Fig. 8b with the propagation velocity over 3000 m/s. The detonation wave presumably originated from the top wall downstream of the fourth obstacle, as deduced from the center of the hemi-spherically expanding detonation wave.

The shock wave “f” in Fig. 8b corresponds to that driven by the flame acceleration (“b” in Fig. 6b). However, the shock wave corresponding to “b” in Fig. 6a is not observed in Fig. 8a. The generation of this shock wave would not

be as reproducible as the generation of the shock wave by the flame acceleration. Based on the images in Fig. 8a, it could not be conclusively demonstrated that transition occurred without the contribution of the shock compression, because the spatial resolution of the images was insufficient to capture in detail the final phase of the transition, and the schlieren images behind the obstacle were superposed with the main flame front. For example, the rapid reaction behind the obstacle, as observed in Fig. 8a, could also have driven the shock wave. The detonation wave originated from the corner bounded by the obstacle and the walls of the combustion channel for all the obstacle heights tested in the present study. This result suggests that the reflection and focusing of the shock wave around the corner created the hot spot, and the origin of the shock wave was the flame acceleration and/or the volumetric explosion behind the obstacle. As described in the previous section, a sufficient volume of the unreacted gas behind the obstacle was considered to be required for the detonation transition, even though the global flame speed was still subsonic, as observed in the present study. The mixing of the unreacted and reacted gas was considered to facilitate the chemical reaction in the vicinity of the flame front interacting with the vortex. The height (5–15 mm) and depth (85 or 100 mm) of the obstacle were used to obtain a rough estimation of the size of the unreacted gas pocket, which was compared to the cell width. This was analogous with the condition required for the jet initiation [14–16], which was often expressed by the orifice diameter and the cell width, and in which the detonation wave was initiated by the turbulent mixing between the unreacted gas and the jet of the combustion products. The height and depth of the obstacle were about 2.5–7.5 times and about 40–50 times greater than the cell width of the initial unreacted gas, respectively. The height was below the order of ten times the cell width, which was the minimum required orifice diameter for the jet initiation [14–16] and the minimum scale required for the detonation onset in the DDT process of fuel–air mixtures [2, 10]. On the other hand, the depth was sufficiently large. This rough estimation supports the idea that the detonation transition could occur behind the obstacle if the proper condition was satisfied, such as the formation of the hot spot by the shock wave. The observations in the present study revealed that the detonation transition could occur in a highly reactive mixture without sufficient flame acceleration in a channel with repeated small obstacles, and also revealed the three-dimensional evolution of the DDT process. However, the flow field after flame propagation around the obstacle was complex and hard to observe in detail due to the spatial resolution limitations of the images. Furthermore, the reason why the obstacle height affected the location of the detonation transition could not be sufficiently addressed in this study. The investigation of the detailed flow phenomena behind each

obstacle remains for future work. In addition, decreasing the initial pressure (reactivity of the mixture) would lead to a change in the mechanism of the detonation transition from that observed in the present study, to one that would occur after flame acceleration beyond the sound speed, as observed in most combustible mixtures. The change of the DDT process arising from the variation of the initial pressure (mixture sensitivity) was outside the scope of the present paper, and remains for future work. Finally, it should be emphasized that the DDT mechanism observed in the present study will occur only in the cases using highly reactive mixtures, such as fuel–oxygen mixtures with high initial pressure. This DDT mechanism is not applicable to conditions relevant to industrial explosion safety, as these situations typically involve a fuel–air mixture at around atmospheric pressure.

4 Conclusions

In this study, the DDT process in a square cross-sectional channel equipped with repeated obstacles was investigated for a highly reactive mixture ($2\text{H}_2 + \text{O}_2$). The conclusions are as follows:

1. A remarkable reduction in the DDT distance was obtained by inserting only three or four repeated obstacles of 5–15 mm height inside the 85 mm \times 100 mm cross-section channel. The DDT distances were reduced to the range of 140–200 mm from the ignition point, compared with 1.0–1.5 m in the case without obstacles.
2. When the repeated obstacles were installed in the highly reactive system, the detonation transition occurred without global flame acceleration beyond the unreacted mixture sound speed. The DDT distance did not change even when the downstream obstacle was removed at the location of detonation onset. This indicated that the detonation onset was dominated by the local condition behind the obstacle where the detonation occurred.
3. The multi-frame schlieren imaging indicated that the interaction of flame and flow field downstream of the obstacle seemed to be important for the onset of detonation. A volumetric explosion was observed in the unreacted gas pocket behind the obstacle when the flame front was convoluted by the vortex. The mixing of hot reacted gas into the unreacted gas pocket was considered to induce the volumetric explosion. The final onset of the detonation originated from the unreacted gas pocket, which was bounded by the obstacle and the channel walls, and a possible mechanism for the detonation initiation was considered to be the volumetric explosion with the formation of a hot spot by the shock wave.

References

1. Lee, J.H.S.: *The Detonation Phenomenon*. Cambridge University Press, New York (2008)
2. Ciccarelli, G., Dorofeev, S.: Flame acceleration and transition to detonation in ducts. *Prog. Energy Combust. Sci.* **34**, 499–550 (2008)
3. Urtiew, P.A., Oppenheim, A.K.: Experimental observation of the transition to detonation in an explosive gas. *Proc. R. Soc. Lond. A* **295**, 13–28 (1966)
4. Shchelkin, K.I., Troshin, Ya.K.: *Gasdynamics of Combustion*. Mono Book Corporation, Baltimore (1965)
5. Ciccarelli, G., Fowler, C.J., Bardon, M.: Effect of obstacle size and spacing on the initial stage of flame acceleration in a rough tube. *Shock Waves* **14**, 161–166 (2005)
6. Johansen, C.T., Ciccarelli, G.: Visualization of the unburned gas flow field ahead of an accelerating flame in an obstructed square channel. *Combust. Flame* **156**, 405–416 (2009)
7. Lee, J.H., Knystautas, R., Chan, C.K.: Turbulent flame propagation in obstacle-filled tubes. *Proc. Combust. Inst.* **20**, 1663–1672 (1984)
8. Peraldi, O., Knystautas, R., Lee, J.H.: Criteria for transition to detonation in tubes. *Proc. Combust. Inst.* **21**, 1629–1637 (1986)
9. Gamezo, V.N., Ogawa, T., Oran, E.S.: Numerical simulations of flame propagation and DDT in obstructed channels filled with hydrogen-air mixture. *Proc. Combust. Inst.* **31**, 2463–2471 (2007)
10. Dorofeev, S.B., Sidorov, V.P., Kuznetsov, M.S., Matsukov, I.D., Alekseev, V.I.: Effect of scale on the onset of detonations. *Shock Waves* **10**, 137–149 (2000)
11. Oran, E.S., Gamezo, V.N.: Origin of the deflagration-to-detonation transition in gas-phase combustion. *Combust. Flame* **148**, 4–47 (2007)
12. Liberman, M.A., Kuznetsov, M., Ivanov, A., Matsukov, I.: Formation of the preheated zone ahead of a propagating flame and the mechanism underlying the deflagration-to-detonation transition. *Phys. Lett. A* **373**, 501–510 (2009)
13. Obara, T., Kobayashi, T., Ohyagi, S.: Mechanism of deflagration-to-detonation transitions above repeated obstacles. *Shock Waves* **22**, 627–639 (2012)
14. Knystautas, R., Lee, J.H., Moen, I., Wanger, H.G.G.: Direct initiation of spherical detonation by a hot turbulent gas jet. *Proc. Combust. Inst.* **17**, 1235–1245 (1979)
15. Carnasciali, F., Lee, J.H.S., Knystautas, R.: Turbulent jet initiation of detonation. *Combust. Flame* **84**, 170–180 (1991)
16. Inada, M., Lee, J.H., Knystautas, R.: Photographic study of the direct initiation of detonation by a turbulent jet. *Prog. Astronaut. Aeronaut.* **153**, 253–269 (1992)
17. Manzhalei, V.I., Mitrofanov, V.V., Subbotin, V.A.: Measurement of inhomogeneities of a detonation front in gas mixtures at elevated pressures. *Combust. Explos. Shock Waves* **10**, 89–95 (1974)
18. Kaneshige, M., Shepherd, J.E.: Detonation database. GALCIT Technical Report FM97-8 (1997)
19. Gu, X.J., Haq, M.Z., Lawes, M., Woolley, R.: Laminar burning velocity and Markstein length of methane-air mixtures. *Combust. Flame* **121**, 41–58 (2000)
20. Sun, Z.-Y., Liu, F.-S., Bao, X.C., Liu, X.-H.: Research on cellular instabilities in outwardly propagating spherical hydrogen-air flames. *Int. J. Hydrogen Energy* **37**, 7889–7899 (2012)
21. Gordon, S., McBride, B.J.: Computer program for calculation of complex chemical equilibrium compositions and applications, NASA Reference Publication 1311 (1994)
22. Kuznetsov, M., Alekseev, V., Matsukov, I., Dorofeev, S.: DDT in a smooth tube filled with a hydrogen–oxygen mixture. *Shock Waves* **14**, 205–215 (2005)